

DEFECT DEPTH-PROFILING IN KESTERITE ABSORBER BY MEANS OF CHEMICAL ETCHING AND SURFACE ANALYSIS

Kunal J. Tiwari¹, Robert Fonoll Rubio¹, Sergio Giraldo¹, Lorenzo Calvo-Barrio^{2,3}, Victor Izquierdo-Roca¹, Marcel Placidi^{1,4}, Yudania Sanchez¹, Alejandro Pérez-Rodríguez^{1,3}, Edgardo Saucedo^{1,4}, and Zacharie Jehl Li-Kao^{1,4*}

1. *Institut de Recerca en Energia de Catalunya (IREC), 1,2^a pl. Jardins de les Dones de Negre, 08930 Sant Adria de Besos, Barcelona, Spain.*
2. *Centres Científics i Tecnològics (CCiTUB), Universitat de Barcelona, C/ Lluís Solé i Sabaris 1-3, 08028 Barcelona, Spain.*
3. *IN²UB, Departament d'Enginyeria Electrònica i Biomèdica, Universitat de Barcelona, C/ Martí i Franquès, 1, 08028 Barcelona, Spain.*
4. *Electronic Engineering Department, Polytechnic University of Catalonia (UPC), c/ Jordi Girona 1, 08034 Barcelona, Spain.*

Keywords: chemical etching; defect; Kesterite; Raman Spectroscopy; XPS

Abstract:

A method to probe the depth morphology, defect profile and possible secondary phases in a thin film semiconductor is presented, taking a standard Kesterite film as an example. Using a top-down approach based on a previously reported controlled Methanol-Br₂ chemical etching, well-defined slabs of a state of the art Kesterite absorber are fabricated. The analysis of their morphology both by Scanning Electron Microscopy and 3D optical Profilometry reveals the extent of a previously reported poor film morphology toward the back interface, and we are able to determine that more than 50% of a standard absorber is disconnected from the substrate. More importantly, these etched films are subsequently analyzed by surface sensitive techniques such as X-ray Photoelectron Spectroscopy and UV-Raman analysis. An accurate composition profile is established, and for the first time, a direct observation of the defects' nature and their depth profiling in Kesterite is made possible. While V_{Cu} are found with a constant amount throughout the absorber, indicating a homogenous carrier concentration, a prevalence of the Zn_{Sn} defect is observed with a steep gradient toward the back interface, associated with an increase in the SnSe₂ secondary phase. With bulk defects being often pointed out as the intrinsic limitation of this material, this result highlights what possibly is the main impediment of Kesterite solar cells, and a critical point to address in the design of future devices. Beyond the case of Kesterite absorbers, the method presented here offers a combination of simplicity, tunability and versatility making a straightforward transfer to other emerging thin film absorbers feasible, and it could possibly be an important tool in their future performance assessment and comparison.

I. Introduction

With several technologies reaching their industrial maturity, thin film solar cells are now credible players in the photovoltaic landscape, reinforced by the need for new applications in fields like Building Integrated Photovoltaics (BIPV) ¹, the Internet of Things (IoT) along with the emerging indoor

photovoltaics systems ². Throughout the development of thin film solar cells, spanning more than 4 decades, material scarcity and toxicity has been an ongoing research axis ³ and the level to which it could hamper the growth of these technologies remains debatable among the photovoltaic community ^{4,5}.

In that context, Kesterite absorbers being free of toxic and critical raw materials were seen (and to some extent still are) as a potential low-cost answer ⁶; disappointingly however, the conversion efficiency of the PV devices has been stalling throughout most of the last decade ⁷⁻⁹, and fundamental limitations challenge further progresses of this technology ¹⁰. Namely, a strong voltage deficit has been identified as the main parameter constraining the performance of Kesterite-based devices ⁸. A recent landmark study ¹¹ even concluded to an upper limit in the efficiency of those imperfect crystals around 20%, mostly ascribed to the presence of native defects in the absorber. The presence of such defects has been long suspected in the community, but their direct observation remains challenging and one has to rely on indirect approaches such as admittance spectroscopy to identify the energy position of defects and infer their nature ¹²; hence the need for a novel approach to this problem. In semiconductor materials for energy application, the lack of easy characterization methodologies compatible with an extensive application in different synthesis conditions is a critical limitation to the understanding of the defects' role, and their engineering would allow for a pathway to device optimization ¹³.

The chemical etching of thin film absorbers using a bromine solution has been a valuable top-down method used in the past to investigate on the possible improvement of the p-n junction ¹⁴ as well as the fabrication of proof-of-concept ultrathin absorbers in CIGSe ^{15,16}, and similar solutions have proven applicable to Kesterite absorbers as well ^{17,18}. In this work, we aim at building upon these past investigations to propose an original yet simple method in the thorough characterization of the defects existing in reference CZTSe Kesterite absorbers. Unlike previous studies, our approach allows for a direct defect observation throughout the whole absorber thickness, by dividing the film into slabs with a bromine etching on reference samples, and using surface sensitive characterizations to build a complete composition and defect profile of the absorber. Chemically etched films will be analyzed by confocal optical 3D Profilometry (3D-P), Scanning Electron Microscopy (SEM), Raman Spectroscopy and X-ray Photoelectron Spectroscopy (XPS), and the morphology of the back side of the absorber will be revealed as a major limiting factor, with a poor crystallinity, several voids, and the presence of various secondary phases; such problems have long been ascribed to poor performances in Kesterite-based solar cells ^{19,20}, and the progressive chemical etching of our absorbers reveals that more than 50% of the surface area of the film is disconnected from the Mo back contact. The analysis of etched absorbers by XPS allows for an accurate composition profiling of the films, revealing features that were not observable in a standard profiling using sputtering. From UV-Raman observations ²¹, a strong prevalence of the Zn_{Sn} deep donor defect is demonstrated, and discussed in regard to previous calculations made on this material ¹¹; it is to the best of our knowledge the first time that such experimental depth-resolved defect profile is established in Kesterite absorbers, and our method allows to directly identify what fundamental limitations to the performance of the resulting PV devices. This work uses a combination of well controlled experimental techniques to provide direct experimental insights on critical aspects of CZTSe Kesterite solar cells which were so far either indirectly inferred or deduced from numerical modelling.

Beyond the issues related to Kesterite solar cells, our method is, to some extent, material agnostic and it can potentially be applied to a wide array of other thin films; it could prove particularly valuable in

the study of emerging materials, as a mean to devise improvement strategies based on their defect profile and the presence of secondary phases in the bulk.

II. Materials and Methods

A. Samples preparation

Kesterite $\text{Cu}_2\text{ZnSnSe}_4$ (CZTSe) films are prepared following the standard process in our laboratory on Soda Lime Glass (SLG) coated by an 800nm layer of molybdenum (Mo). A Cu, Zn and Sn metallic precursor with the elemental layer stack order Cu/Sn/Cu/Zn is first deposited by sequential DC sputtering (Alliance concept AC450), and the semiconductor film is realized by a 2-steps thermal annealing in a tubular furnace (Hobersal) in the presence of the chalcogen element Se. In a first step, the sample was heated to 400°C for 30min under a constant Ar flow of 1.5mbar; in a second step, the temperature was ramped up to 550°C and a static Ar pressure of 950mbar was maintained, for a total of 15min. The as-selenized film was 3 μm thick for this work, thicker than our usual absorbers. This is the only variation with the standard process, and it was deemed useful in the context of a top-down approach to use thicker films. While beyond the scope of this study, a complete solar cell using the as-deposited 3 μm absorber was fabricated, with a conversion efficiency on par with the expectation of a reference sample. Additionally, the etching of thinner standard absorbers was also performed and a more limited analysis of these samples brought similar observations to what is discussed in this study, confirming that using thicker absorbers should not change our conclusion. Hence, we make the choice to discuss our experiments on 3 μm thick CZTSe films, providing here a more exhaustive analysis. No additional treatment is done prior to the etching of the films.

B. Bromine etching process

Bromine etching is a previously reported method¹⁴ to effectively reduce the thickness of metallic and semiconductor thin films without altering their properties, and the demonstration of its effectiveness was previously made on CIGS^{15,22}. While the most widely reported method involves H_2O and HBr along with Br_2 , we chose to use a Methanol- Br_2 solution for practical reasons¹⁷, which yields equivalent results. The Br_2 concentration was 0.02M, and the etching was carried out with a controlled temperature close to 0°C by maintaining the etching vessel in an ice bath 10 minutes before dipping the samples in the solution, as well as during the etching process. Unless specified otherwise, no additional treatment to the samples was done after etching. The samples were kept in a vacuum environment and characterized less than 12h following the etching process. A series of 9 samples was fabricated (including a reference non-etched sample), with etching durations for 8 samples ranging from 30sec up to 13min, the latter corresponding to an etched thickness >2 μm , though we will later see that determining an etched thickness is not straightforward when approaching the back contact. The etched samples are numbered from 1 to 9, with #4 being deliberately excluded from the series. A special emphasis was put on short etches, for reasons detailed later in the manuscript.

C. Samples characterization

The characterization process of as deposited and etched samples in this study is fully contactless. The films are characterized by Zeiss series Auriga scanning electron microscope (SEM) with accelerating voltage of 5 kV and X-ray fluorescence (XRF, *FISCHERSCOPE XDV*) to allow determining their thickness, and having a direct observation of their morphology change from the bromine etching. 3D Optical Profilometry (3D-P) is used to obtain numerical values related to the surface smoothing post Br₂ etching, and the film composition for different etching durations is monitored by XRF. All XRF data reported are the average values obtained on 9 different positions on the samples.

UV-Raman analysis is performed on as-deposited and etched samples using a 325nm excitation wavelength and an in-lab developed Raman system with an extremely low power density (<60W/cm²) to avoid thermal effects and alterations, and a large laser diameter spot (70μm) covering a representative area of the sample. This latter point is also critical in our opinion, as the observations reported here are thus more representative than what a local analysis would provide. Working under UV conditions allows for a light penetration depth below 10nm while non-bandgap resonance Raman conditions enhance the detection of peaks sensitive to V_{Cu} and Zn_{Sn} type defects²¹. The samples were stored in vacuum conditions and analyzed by Raman less than 24 hours after the chemical etching.

X-ray Photoelectron Spectroscopy (XPS) experiments are performed in a PHI 5500 Multitechnique System from Physical Electronics, using a monochromatic X-ray source Al K α line of 1486.6eV energy and 350W power, placed perpendicular to the analyzer axis and calibrated by the 3d_{5/2} line of Ag with a full width at half maximum (FWHM) of 0.8eV. The analyzed area is a circle of about 0.8mm diameter. The selected resolution for the survey spectra (from 0 to 1100eV of binding energy) is 187.5eV of Pass Energy (PE) and 0.8eV/step. For the high-resolution spectra 23.5eV of PE and 0.1eV/step are chosen to measure the main orbitals of Kesterite's elements (Cu2p, Zn2p_{3/2}, Sn3d and Se3d), Molybdenum (Mo3d), Carbon (C1s) and Oxygen (O1s). Due to this large number of existing elements, overlaps will appear between some of the signals that must be considered to avoid confusion (more explained in Supporting Information).

Besides, in-depth measurements (profiles) are obtained in the reference sample by sputtering it with an Ar⁺ ion source (3.5keV). One profile following only Mo3d signal is run to know the sputter ratio, and a second profile for all CZTSe elements, Mo and O main orbitals with the same parameters of high-resolution spectra is done to compare with the obtained data on the bromine etching samples.

The analysis and fitting of the XPS spectra are done with Multipak Version 9.9.08 program from ULVAC-PHI. Measurements are referenced to the C1s signal, which binding energy is equal to 284.8eV in adventitious Carbon (from atmospheric contamination). For quantification purposes, the corrected relative sensitivity factors provided by the same program are used. These factors consider both the specific analyzer parameters and the geometry of the experimental system. No charge compensation is used in any of these measurements that are made in an ultra-high vacuum (UHV) chamber, with pressures between 1x10⁻⁹ and 2x10⁻⁸ torr.

III. Results and discussion

A. Samples' morphology and interplay with the etching process

The effect of bromine etching on the morphology of CIGSe absorbers has been widely reported^{14,15,22}, and a strong smoothing effect with RMS values below 50nm was observed in previous studies from Atomic Force Microscopy (AFM) analysis. A similar statement was anecdotally made on CZTSe¹⁷ but the morphology of the films was beyond the scope of this aforementioned study. We deem necessary to confront and confirm those results, and this work starts by investigating the evolution of the surface roughness of CZTSe films and its interplay with the etching kinetics. Optical Profilometry (3D-P) is preferred to AFM in our case, as we aim at analyzing a surface area as representative as possible of the sample; however, one may keep in mind that this approach has the drawback of a comparatively lower resolution (in our case of the order of 10-20nm). Moreover, a higher RMS value is expected when using 3D-P as compared to AFM (as done in previous studies), as a larger area is being analyzed; hence, a direct 1:1 comparison with the previous AFM work on CIGSe is not advisable, and only trends should be considered.

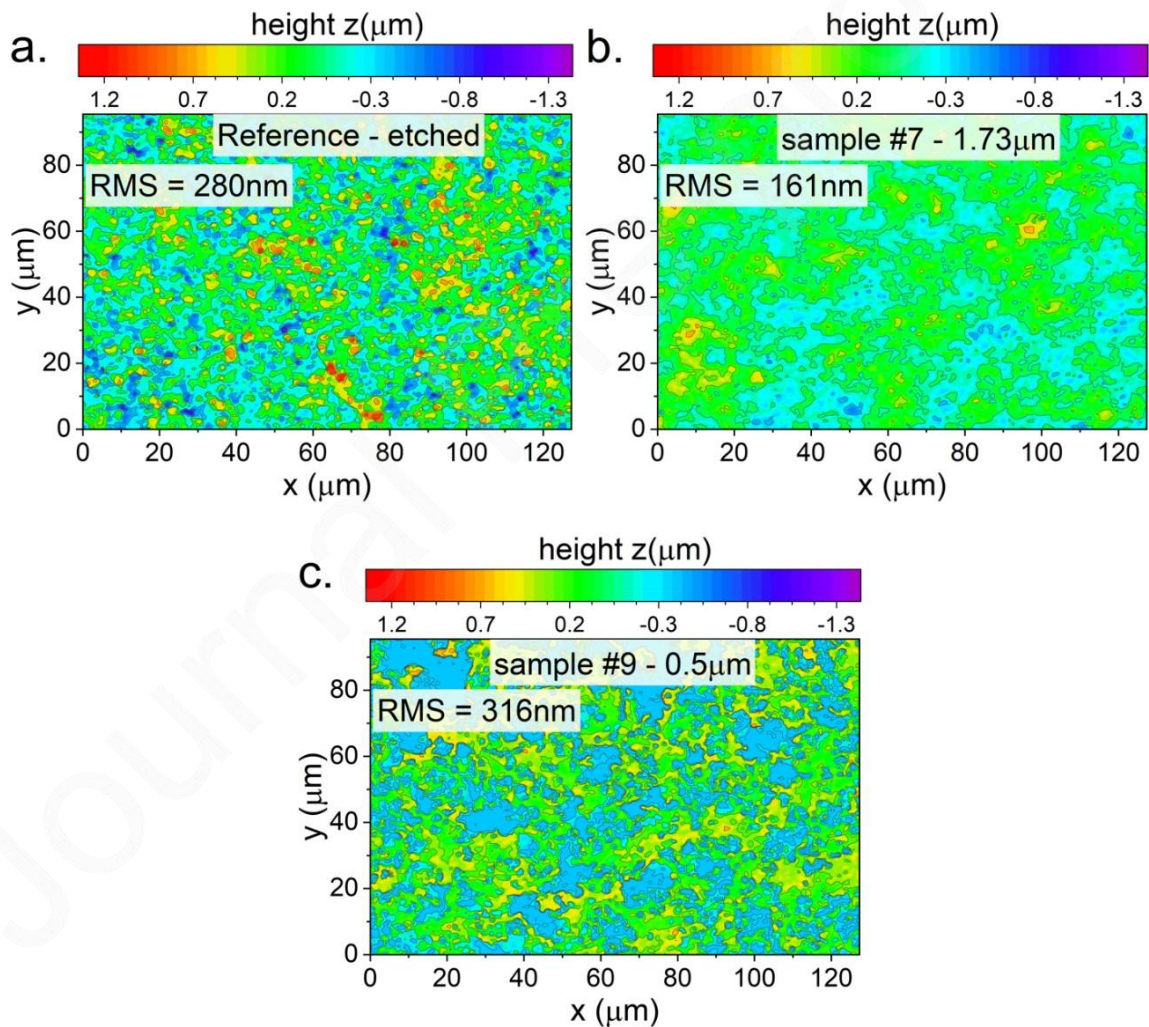


Figure 1 Surface profile of the reference non-etched CZTSe film (a) and differently etched samples (b and c), representative of the evolution of the surface roughness.

Figure 1a, Figure 1b and Figure 1c show the surface profile of 3 selected CZTSe samples with different etching durations; the evolution of the surface RMS and etching rate are shown in the supplementary information of this manuscript, as those would not qualify as new results since similar trends have been observed on CIGSe²². The reported thickness (remaining sample thickness) was measured by XRF analysis; due to the textured nature of the samples, which makes the concept of thickness somehow inaccurate, this value should rather be seen as indicative of the quantity of material being removed from the sample. A clear decrease in the surface roughness is observed, starting from $\approx 300\text{nm}$ for the reference non-etched sample Figure 1a down to a minimum of 160nm for three consecutive samples etched for 240s, 360s and 540s (corresponding to a remaining thickness of $2.27\mu\text{m}$, $2.07\mu\text{m}$ and $1.73\mu\text{m}$ respectively as shown Figure 1b). For longer etching durations, a strong increase in the RMS value is observed; concurrently, large and very flat areas (in light blue in Figure 1c) appear on the 3D-P images (Figure 1c). These areas correspond to the bare Mo surface, and are thus indicative of very large voids existing at the back side of the films. An image analysis shows that up to 50% of the Mo surface is disconnected from the CZTSe film, which is a severe limitation to the performance of solar cell devices. Similar observations have been made in the recent years and were recently attributed to a wettability mismatch at the back interface²³. The images presented Figure 1 provide here a direct observation of the extent to which this issue affects Kesterite absorbers, and it is the main novelty of the morphological analysis permitted through chemical etching. In the future, a similar analysis of samples fabricated with strategies addressing this specific issue (see reference²⁰) could prove valuable in assessing possible improvements at the back interface. Though beyond the scope of this work, a mechanical lift-off was performed on a different series of CZTSe samples revealing similar features as those observed here; this specific point will be thoroughly addressed in a future study.

The etching rate is calculated from the XRF analysis of the samples, and is presented Figure SI 1. Two seemingly linear rates coexist; a fast etching rate for the first 500nm , followed by an approximately 30% slower rate. As the etching rate should remain constant in terms of quantity of etched material, the limiting parameter is the exposed film total area; such behavior is therefore consistent with a rapid smoothing of the film's surface, and expected as similar results were reported on CIGS¹⁵. Consistently with the presence of voids at the back side, a "3D" surface is quickly formed for deeper etchings, increasing the exposed film area and thus accelerating the apparent etching rate; it is also possible that the presence of secondary phases will influence the etching kinetics, though only few experimental points are available here. This specific aspect will need a more thorough analysis in the future before any conclusion can be made. While the chemistry of the etching was discussed elsewhere^{14,17} and is out of the scope of this study, this simple process combined with a surface profiling gives a direct visual and quantitative representation of a major limitation of standard Kesterite absorbers.

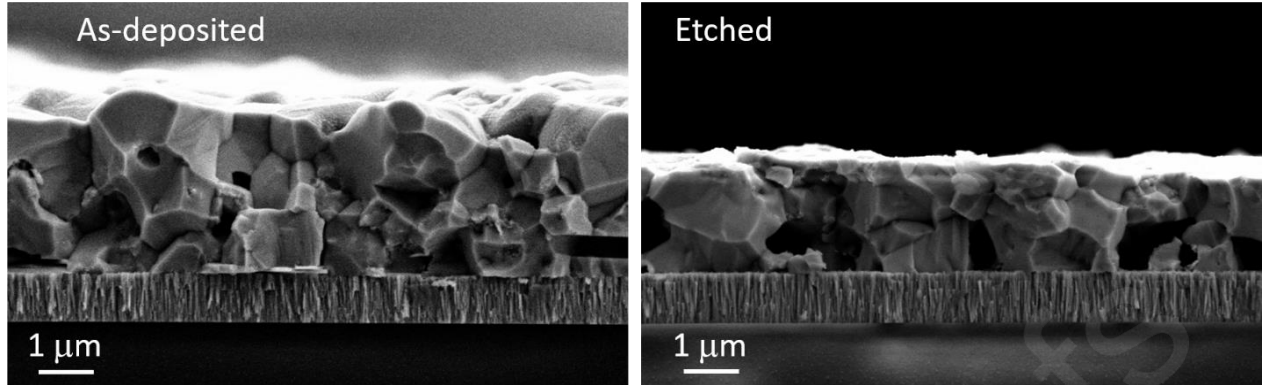


Figure 2 Scanning Electron Microscopy images of the cross sections for the reference non-etched sample (top) and sample #6 (bottom, 360s etching duration). Both images are taken at 30k magnification.

The observation of the layers by cross-sectional SEM (Figure 2, comparing the reference sample with an etched one) reveals consistent information with the previously discussed points; though they do not allow to assess the full extent of the back contact issue, voids and a poor morphology are observed at the back interface between CZTSe and Mo. The smoothing effect from the chemical etching is also visible, though again, a full assessment is only possible through the 3D-P analysis. No apparent damage from the chemical etching are observed on the SEM images.

The etching process of Kesterite films resembles that of chalcopyrite, and in that context, we believe that it could also be used to fabricate complete solar cell devices with a new degree in tailoring the front interface's morphology and render it more specular. In this study however, our main focus remains the composition and defect profiling of a standard CZTSe film, and a point which will be addressed in the following main part of this work.

B. Composition and defects' profiling

The investigation of these samples by XPS is not straightforward, and to justify an appropriate approach, three different methods are considered: direct characterization of as-deposited samples (raw), after surface cleaning using ethanol and N₂ dry-off (ethanol cleaned), and after a light sputtering of the surface (sputtered) using Ar⁺ ions inside the Ultra High Vacuum chamber for half a minute, leading to an erosion below 10 nanometers.

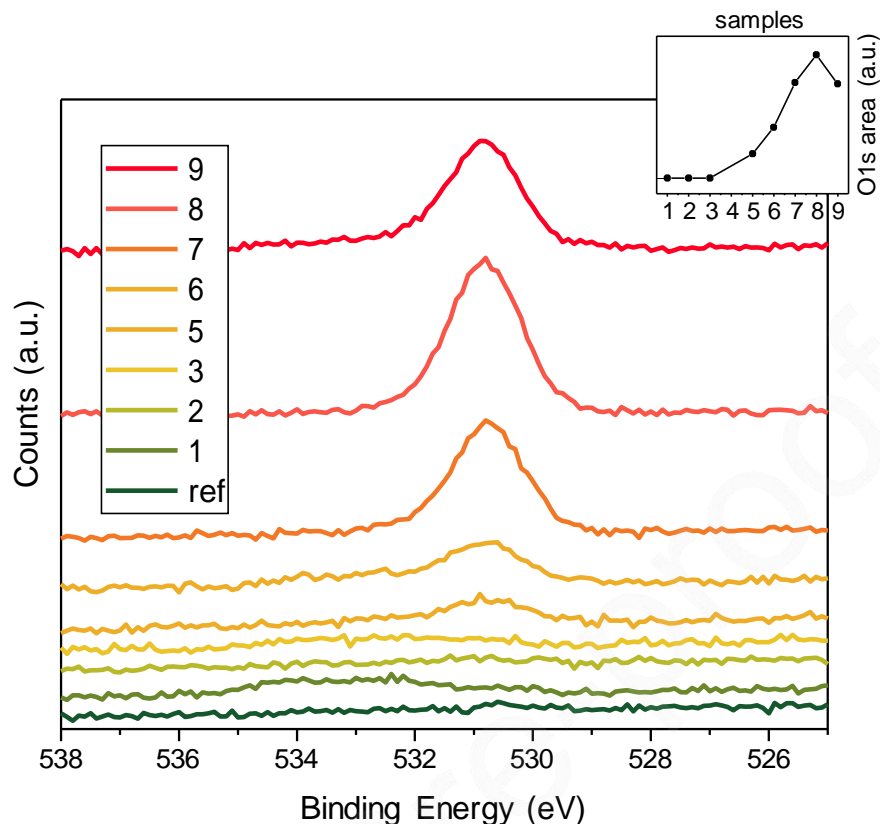


Figure 3 Evolution of the O1s orbital measured by XPS in the complete sample series.

Survey and high-resolution results (figures for raw and sputtered samples are presented in the Supporting Information) show that no real differences can be appreciated between raw and ethanol cleaned measurements, as similar quantities of carbon (C1s) and oxygen (O1s) and no apparent differences in the rest of the Kesterite elements are found. The sputtered measurements show the total disappearance of C1s signals, which is consistent with an adventitious carbon contamination from the air exposure of the samples. The O1s signal however did not fully disappear after sputtering, even though it would have been expected in the case of an atmospheric contamination; it is thus likely that O exists in some form in the film, while C does not. Figure 3 shows the evolution O1s peaks and its relative amount for the different etched samples after sputtering; here, the samples will be referred to by their ascribed number rather for clarity reasons. This amount of oxygen is probably oxidizing a metal, being Sn and Mo the best candidates as it would be shown later. Moreover, Kesterite individual elements for sputtered samples show the expected signal incremental evolution with respect to the raw spectra from the elimination of the surface contamination. Measurements performed on sputtered samples were, for that reason, chosen for quantification purpose.

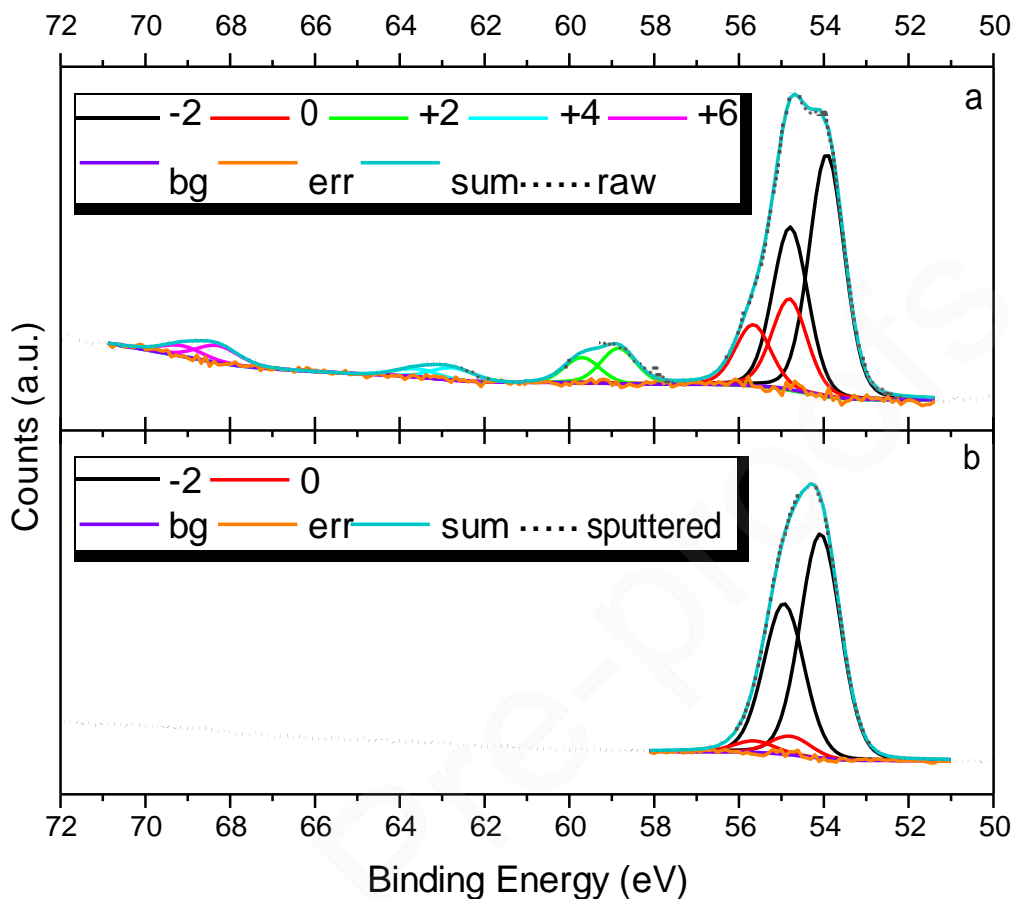


Figure 4 a: XPS Se3d orbital analysis and fit for raw sample #7. b: similar analysis with sputtered sample #7.

On the other hand, the high-resolution Kesterite spectra of sputtered samples show notable changes in shape, FWHM and binding energy with respect to the raw samples. This effect is clearly visible in Figure 4 where Se3d orbital for raw (a) and sputtered (b) measurements together with their detailed fit are shown for sample #7 as an example (a similar conclusion was made on other samples). There exist 5 different bonds (each being a doublet) on the raw sample, among which 3 disappear after the sputtering. The disappearing bonds at about 59, 63 and 68eV can be matched to the different types of oxidation states +2, +4 and +6 respectively, and are routinely observed on surfaces including elemental Se²⁴. The remaining bonds at about 55 and 54eV are related to 0 (elemental) and -2 (as in Kesterite) states. However, the ratio between these 2 remaining bonds changes clearly after the sputtering and the amount of 0 state notably decreases, showing a significant alteration (reduction), of the chemical bonding from sputtering. Hence, it is conversely preferred to refer to the raw measurements for the analysis, fit, and subsequent study of the possible changes in chemical bonding occurring between the differently etched samples.

From the analysis of the area of the peaks corresponding to the different CZTSe elements on all the sputtered samples, and using the corresponding corrected relative sensitivity factors, the atomic concentration profile for CZTSe elements and Mo of Figure 5a is created. In this figure, the expected

composition of a stoichiometric Kesterite is obtained for the reference non-etched sample, but as the etching progresses, the Sn profile begins to increase and reaches a maximum at about 1 μm in remaining thickness, decaying at 0.5 μm . This tin enrichment matches well with the appearance of SnSe₂ peaks on the Raman spectra, as will be later discussed. The molybdenum unsurprisingly appears for the deepest etching, while the Sn content decreases as less material remains scattered on the surface (see Figure 1c). The decrease in both Se and Sn as Mo appears in the profile is consistent with a previously made hypothesis that the voids at the back interface are the result of the evaporation of Sn-Se phases²⁰. This profile should be compared to the in-depth profile obtained directly from the reference sample using a more standard sputtering etching (Figure SI 5 shown in the Supporting Information). In that case, every element displays a more stable and homogenous behaviour until the appearance of molybdenum and no depth tin enrichment is observed. Specifically, the Zn/Sn ratio appears constant in Figure SI 5, while the composition analysis obtained from the chemically etched samples Figure 5a highlighted a strong Sn enrichment from the surface to the Mo back interface, and thus a decrease of the Zn/Sn atomic ratio. We believe that the difference observed when using a standard sputtering etching stems from the confluence of a very long sputter time (continuous damage in bulk by the Ar⁺ ions) and a relatively big area of measurement (the data could be disrupted by the walls of the created crater), usually giving as a result similar homogeneous profiles and losing finer information in deeper layers. The approach chosen in our study, using a soft chemical etching of the surface over a large area, presents apparently a superior element resolution when it comes to depth composition profiling, and allows a more accurate identification of possible grading such as Sn in this specific case. An overview over a larger number of samples would however be necessary to fully confirm this hypothesis.

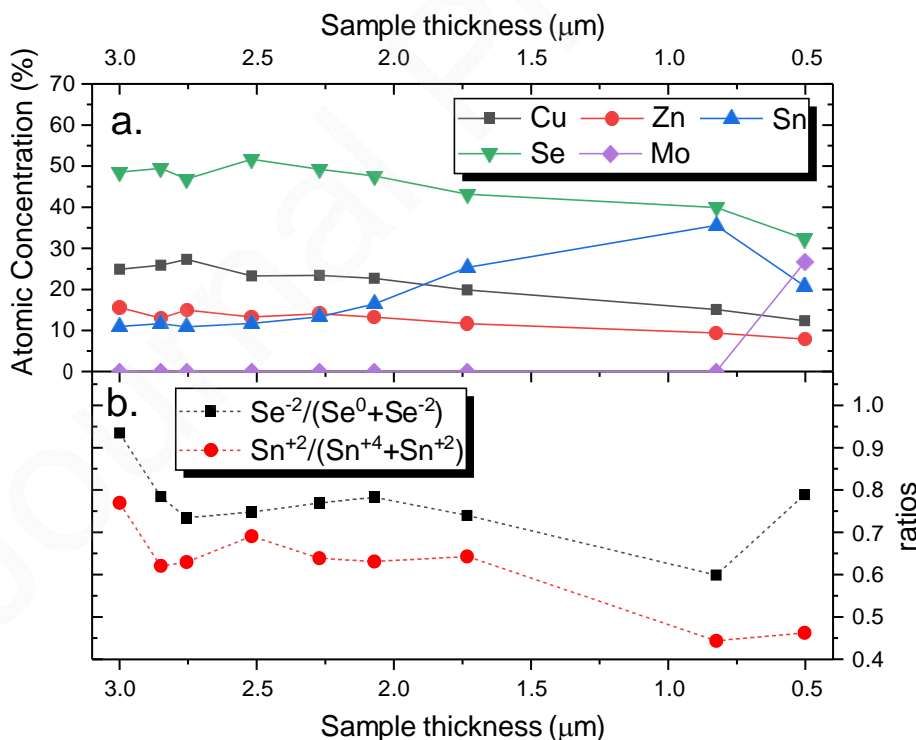


Figure 5 a: Composition profile obtained from XPS analysis of chemically etched samples after a light Ar⁺ sputtering (sputtered).
 b: Sn and Se chemical state ratio evolution on chemically etched samples (raw).

For the analysis of the Kesterite elements' bounds on the etched samples, high-resolution spectra of the raw samples have been analyzed. No significant differences are found on $\text{Cu}2p_{3/2}$ and $\text{Zn}2p_{3/2}$ orbitals for deeper etchings. Both orbitals can be fitted with peaks at about 932.0eV and 1021.8eV. On the other hand, $\text{Se}3d$ and $\text{Sn}3d_{5/2}$ orbitals need to be fitted with different chemical species to reach an acceptable agreement. $\text{Sn}3d_{5/2}$ can be fitted with peaks at about 486.7 and 487.4eV, matching the +2 and +4 chemical species respectively ²⁵. While five doublets are used for the fitting of $\text{Se}3d$, only two of them, corresponding to 0 and -2, are not related with oxidized states typical of a surface atmospheric contamination. Figure 5b shows the ratio between the aforementioned different chemical species for Sn and Se elements for all the etched samples. In the case of selenium, the curve shows that the major bound is always -2, as expected in Kesterite, with a ratio close to 1 at the vicinity of the as-deposited surface. As the etching progresses toward the middle of the layer, a steady regime is reached with a quarter of the selenium appearing elemental. This elemental selenium could have been created around secondary phases present in the sample or around oxidized areas in contact with the voids shown in Figure 1c. When molybdenum appears in the composition profile, we observe an increase in the -2 bond, which can thus easily be ascribed to the presence of MoSe_2 . The tin ratio between the +2 and +4 species follows a similar pattern. While +4 is the stoichiometric state for Kesterite and SnSe_2 secondary phase, +2 also appears in non-stoichiometric samples, and could be an indirect way to identify the appearance of SnSe_x , SnO_x secondary phases or the evidence of defects in the structure ²⁶.

While the approach to combine Br_2 etching with XPS for composition profiling brings valuable information, the investigation of the defects throughout the material is of utmost importance when it comes to assess the current limitations of Kesterite solar cells. A UV-Raman method was recently developed by our group to analyze the surface defects in CZTSe solar cells ²¹, using a non-bandgap resonant effect observed under 325nm excitation conditions. This non-destructive approach allows for an accurate determination of the surface defects, and combined with a systematic chemical etching, it should permit to establish a semi-quantitative defect profile of the material throughout the entire film thickness.

Figure 6 shows the 325 nm Raman spectra of all measured samples (a) and the area ratio of different peaks evaluated from the fitting of the spectra with a lorentzian curve (b). The deconvolution for all samples is shown in the supplementary information Figure SI 6. A clear change of the Raman spectrum is visible with the increased etching duration, previously ascribed to defect concentration variations within the Kesterite structure ²¹ and to the presence of secondary phases ²⁷. The analysis of the Raman spectra with the increase of the etching time shows:

- No evidence of changes in the intensity of the peak at $174\text{-}176\text{ cm}^{-1}$, previously ascribed to the formation of the V_{Cu} point defect linked with the formation of the A-type defect cluster $[\text{Zn}_{\text{Cu}} + \text{V}_{\text{Cu}}]$ ²¹. As Cu vacancies are often ascribed to the carrier concentration in the material, this tends to indicate a homogeneous distribution in that regard.
- An increase of the area of the $245\text{-}250\text{ cm}^{-1}$ peak toward the back interface, previously associated to an increase of the Zn_{Sn} point defect (formation of the B-type defect cluster $[2\text{Cu}_{\text{Zn}} + \text{Zn}_{\text{Sn}}]$) ²¹. This observation is consistent with the low crystalline quality observed in this region by SEM; it also correlates with a prevalence of the SnSe_2 secondary phase, thus reducing the amount of Sn in the Kesterite film.

- A strong accumulation of SnSe₂ phase at the absorber/Mo interface, along with a slight presence at the front surface. In the bulk, the contribution observed is related to tails of the CZTSe peaks suggesting an absence or low concentration of this phase. This observation is also consistent with the SEM observations, XPS analysis and with previous studies on that specific issue²⁰. It also aligns well with a lower incorporation of Sn in the matrix leading to the formation of the Zn_{Sn} point defect.

- A simultaneous detection of a strong signal of the MoSe₂ phase and CZTSe phase in the samples with higher etching time, again consistent with the pinholes observed at the absorber/Mo interface. For those samples, it is evident that part of the signal comes directly from the exposed Mo/MoSe₂ substrate. It should be noted that this MoSe₂ signal is only recorded for the 3 samples with the longer etching durations, and while a logical increase is observed, more experimental points would be necessary to discuss about a trend in that context. Figure 6b illustrates the depth profile of each defect and secondary phase previously discussed. This is to the best of our knowledge the first direct in-depth characterization and experimental semi-quantitative profiling in Kesterite absorbers of such structural imperfections, and it constitutes the highlight of this work.

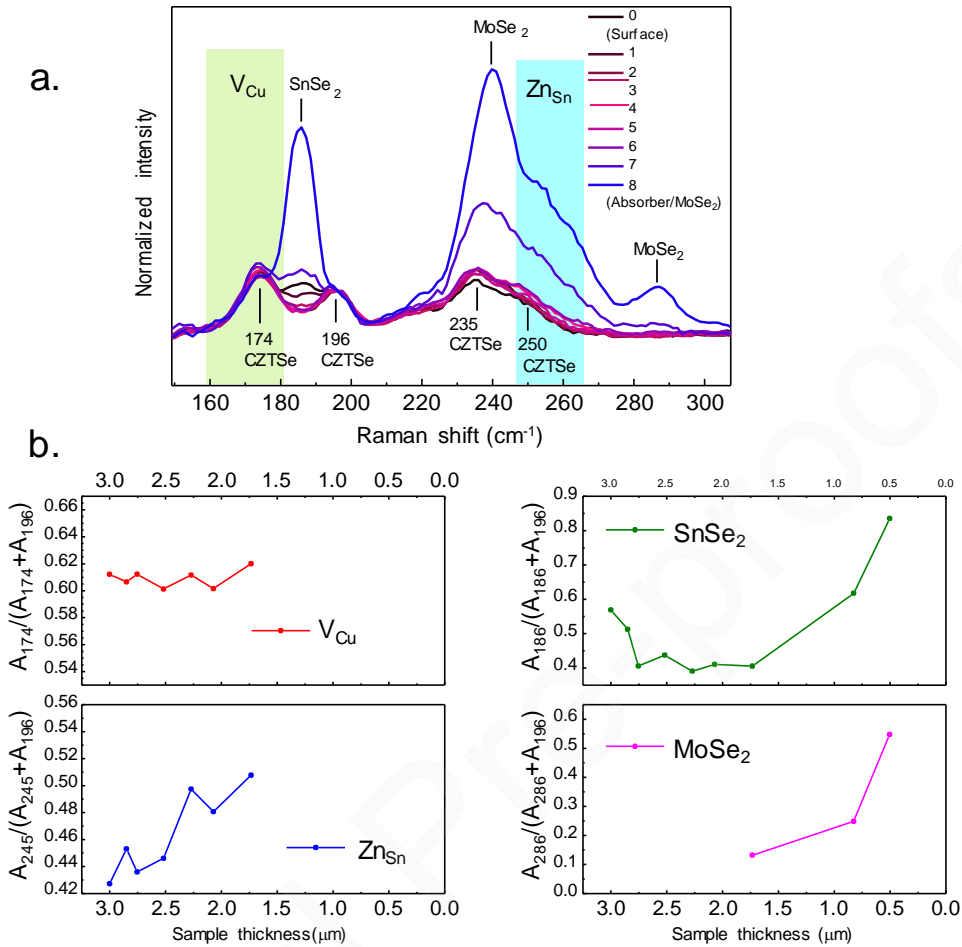


Figure 6 a. Raman spectra using 325 nm excitation wavelength for etched samples. b. Evolution of the integrated area under the peaks associated with the point defects V_{Cu} , $ZnSn$, and the secondary phases $SnSe_2$ and $MoSe_2$.

C. Discussion, limitations and improvement pathways

The novelty of this work lies in the determination of an accurate defect and composition profile using only surface sensitive methods combined with chemical etching. As we investigate Kesterite films produced with the standard process from our laboratory, one should keep in mind that the results obtained are possibly specific to our fabrication method. There is also a possibility that some of the observed defects are either created or affected by the chemical etching; there are however several arguments which tend to demonstrate otherwise. Firstly, the creation of surface defects following a Br_2 etching of chalcogenide films has never been reported, and reference ¹⁴ specifically states that etched surfaces are well defined. Similarly, the fabrication of solar cells on etched absorbers ^{16,22} does not indicate the creation of surface defects. The results from the UV Raman analysis compared with the literature yield very consistent conclusions. In a study from 2013 ²⁸, Chen et al. predicted the prevalence of Sn and Zn related defects, though Sn_{Zn} in cluster with $(2)Cu_{Zn}$ was reported at that time; while we report instead the Zn_{Sn} point defect, it was demonstrated in reference ²¹ that such defect naturally

occurs in a slightly Sn poor Kesterite structure. The prevalence of Sn-related secondary phases tends to confirm that less Sn is incorporated in the absorber. Therefore, it is very unlikely that the defect profile observed in this study results from the Br₂ etching process. Similar defects have recently been identified as directly responsible for the poor carrier lifetime in Kesterite solar cells¹¹ and are in all likelihood the main reason for the high V_{oc} deficit observed in solar cells. Our analysis allows for a direct experimental demonstration of this limitation and a quantitative defect profiling could even be feasible when combined with other characterizations such as admittance spectroscopy, or through the numerical modeling of complete solar cells. Several solutions have been proposed to offset this limitation such as alkali doping or substitution of Cu by Ag, which could potentially help significantly decreasing the concentration of Sn/Zn related defects; this is however beyond the scope of this study, though the method proposed here is fully applicable to the characterization of such films.

The smoothing effect of the chemical etching on chalcogenide films is not a new result; our method allows however to analyze the morphology of the back side of the layer, which is arguably the second most important limitation of Kesterite absorbers. It is however not trivial to assess the extent to which it will degrade the performances. The presence of defects and secondary phases can potentially pin the fermi level below the bandgap and severely hinder the voltage of the solar cells. Back contact recombination may also be an issue despite the high absorption coefficient of the material. Considering the thickness of standard absorbers however (1.5 μm), back contact recombination has regularly been observed in quantum efficiency curves. Strategies are currently being developed in our laboratory with a significant improvement of the back interface morphology [Giraldo et al., *in preparation*, 2020]. Among the methods used to assess those samples, Br₂ etching of the films is a valuable asset in that regard.

The current study lacks data to investigate on the possible interplay between the films' morphology and the surface composition. As shown Figure SI 1, three regimes seem to co-exist when etching a Kesterite film, related to the surface roughness of the layer. A link could possibly exist with the surface composition of the films in the case of selective etching; specifically, if a different etching kinetic exists between the Kesterite and the secondary phases, as illustrated Figure 5b. At this stage, we do not believe however that such interplay exists, as it was not reported in previous studies and the smoothing effect of the etching tends to indicate a homogeneous reaction; this point is specifically addressed in reference²⁹, albeit on CIGSe films rather than Kesterite. Also on CIGSe, Canava et al. showed that an ultrathin layer of elemental Se can be detected at the sample's surface following the etching, though a KCN treatment prior to the buffer layer deposition allows to fully eliminate this layer¹⁴. Additional experiments would be needed before drawing a conclusion in that regard.

The approach proposed in this work was successfully applied to both CIGSe and CZTSe, and preliminary results from our laboratory suggest that Br₂ etching could possibly be used on emerging PV absorbers such Sb₂Se₃. While this reinforces our hypothesis that our method is to an extent material agnostic, it may still be too early to qualify it as such and we hope that the community will contribute in the future with assessing other materials in a similar approach.

Nevertheless, the use of chemical etching combined with surface sensitive characterization methods sheds light on what we believe to be the two main limitations in state of the art CZTSe absorbers, namely a poor back interface morphology, and the prevalence of the Zn_{Sn} point defect, allowing for a direct observation of both.

IV. Conclusion

A method for in-depth analysis of thin film photovoltaic absorbers is proposed and applied to CZTSe Kesterite films. A well-known Br₂ based chemical etching is used and the morphology of etched samples is assessed by surface profiling revealing a smoothing effect similar to previous reports on CIGSe. More importantly, deeper etchings illustrate the extent of the poor back interface morphology of standard CZTSe films, with numerous voids and up to 50% of the Mo surface not directly contacted by the absorber.

A depth-composition analysis of the films by successive chemical etchings and XPS reveals finer details in the elemental profile of the layer, and a specific Sn enrichment toward the back interface is observed; such important feature was not visible when following the standard profiling method in reference sample with a long sputter time, which leads to conclude to a much better accuracy of our approach in that context. The bonds analysis of the Se and Sn elements reveals an increasing occurrence of Se⁰ consistent with a decline in film quality at the back interface, and the presence of both Sn⁺⁴ and Sn⁺² could be an indirect way to identify the appearance of secondary phases and defects in the Kesterite structure.

The UV-Raman analysis of etched samples reveals the prevalence of the Zn_{Sn} defect throughout the absorber thickness, ascribed to the limited carrier lifetime and high V_{oc} deficit typically observed in Kesterite solar cells; on the other hand, V_{Cu} is found mostly unchanged throughout the bulk of the film, indicating a homogenous carrier concentration profile. Finally, tin-related secondary phase SnSe₂ is found increasingly prevalent toward the back interface of the film, which aligns well with the poor morphology observed both by electronic microscopy and confocal surface analysis, as well as the depth-composition profile established using XPS.

The results presented here, obtained on large sample areas, are the first direct observation of the nature and relative profile of defects in CZTSe absorber, highlighting several limitations of this material when fabricated in standard conditions, and providing a valuable insight for the design of future improvement strategies. This approach also holds implications for the entire field of thin films, and it possibly paves the way to both an exhaustive and simple assessment of emerging photovoltaic absorbers, for which the intrinsic limitations remain debatable.

Acknowledgements

This work is possible thanks to the funding from the Ministry of Science and Innovation of Spain under IGNITE project (ENE2017-87671-C3-1-R), the European Regional Development Funds (ERDF, FEDER Programa Competitivitat de Catalunya 2007–2013) and CERCA Programme / Generalitat de Catalunya. Authors from IREC belong to the SEMS (Solar Energy Materials and Systems) Consolidated Research Group of the “Generalitat de Catalunya” (Ref. 2017 SGR 862).

This project has received funding from the European Union’s Horizon 2020 research and innovation programme under the Marie Skłodowska-Curie grant agreement No 712949 (TECNIOspring PLUS) and the Government of Catalonia’s Agency for Business Competitiveness (ACCIÓ).

M.Placidi thanks the Government of Spain for the Ramon y Cajal Fellowship (RYC-2017-23758).

V. References

- (1) Pagliaro, M.; Ciriminna, R.; Palmisano, G. BIPV: Merging the Photovoltaic with the Construction Industry. *Progress in Photovoltaics: Research and Applications* **2010**, *18* (1), 61–72. <https://doi.org/10.1002/pip.920>.
- (2) Mathews, I.; Kantareddy, S. N.; Buonassisi, T.; Peters, I. M. Technology and Market Perspective for Indoor Photovoltaic Cells. *Joule* **2019**.
- (3) Fthenakis, V. Sustainability of Photovoltaics: The Case for Thin-Film Solar Cells. *Renewable and Sustainable Energy Reviews* **2009**, *13* (9), 2746–2750. <https://doi.org/10.1016/j.rser.2009.05.001>.
- (4) Candelise, C.; Winkler, M.; Gross, R. Implications for CdTe and CIGS Technologies Production Costs of Indium and Tellurium Scarcity. *Progress in Photovoltaics: Research and Applications* **2012**, *20* (6), 816–831. <https://doi.org/10.1002/pip.2216>.
- (5) Duan, H.; Wang, J.; Liu, L.; Huang, Q.; Li, J. Rethinking China's Strategic Mineral Policy on Indium: Implication for the Flat Screens and Photovoltaic Industries. *Progress in Photovoltaics: Research and Applications* **2016**, *24* (1), 83–93. <https://doi.org/10.1002/pip.2654>.
- (6) Delbos, S. Kesterite Thin Films for Photovoltaics : A Review. *EPJ Photovolt.* **2012**, *3*, 35004. <https://doi.org/10.1051/epjpv/2012008>.
- (7) Wallace, S. K.; Mitzi, D. B.; Walsh, A. The Steady Rise of Kesterite Solar Cells. *ACS Energy Lett.* **2017**, *2* (4), 776–779. <https://doi.org/10.1021/acseenergylett.7b00131>.
- (8) Giraldo, S.; Jehl, Z.; Placidi, M.; Izquierdo-Roca, V.; Pérez-Rodríguez, A.; Saucedo, E. Progress and Perspectives of Thin Film Kesterite Photovoltaic Technology: A Critical Review. *Advanced Materials* **2019**, *31* (16), 1806692. <https://doi.org/10.1002/adma.201806692>.
- (9) Wong, L. H.; Zakutayev, A.; Major, J. D.; Hao, X.; Walsh, A.; Todorov, T. K.; Saucedo, E. Emerging Inorganic Solar Cell Efficiency Tables (Version 1). *J. Phys. Energy* **2019**, *1* (3), 032001. <https://doi.org/10.1088/2515-7655/ab2338>.
- (10) Siebentritt, S. Why Are Kesterite Solar Cells Not 20% Efficient? *Thin Solid Films* **2013**, *535*, 1–4. <https://doi.org/10.1016/j.tsf.2012.12.089>.
- (11) Kim, S.; Márquez, J. A.; Unold, T.; Walsh, A. Upper Limit to the Photovoltaic Efficiency of Imperfect Crystals from First Principles. *Energy Environ. Sci.* **2020**. <https://doi.org/10.1039/D0EE00291G>.
- (12) Kask, E.; Grossberg, M.; Josepson, R.; Salu, P.; Timmo, K.; Krustok, J. Defect Studies in Cu₂ZnSnSe₄ and Cu₂ZnSn(Se_{0.75}S_{0.25})₄ by Admittance and Photoluminescence Spectroscopy. *Materials Science in Semiconductor Processing* **2013**, *16* (3), 992–996. <https://doi.org/10.1016/j.mssp.2013.02.009>.
- (13) Li, G.; Blake, G. R.; Palstra, T. T. Vacancies in Functional Materials for Clean Energy Storage and Harvesting: The Perfect Imperfection. *Chemical Society reviews* **2017**, *46* (6), 1693–1706.
- (14) Canava, B.; Guillemoles, J. F.; Vigneron, J.; Lincot, D.; Etcheberry, A. Chemical Elaboration of Well Defined Cu(In,Ga)Se₂ Surfaces after Aqueous Oxidation Etching. *Journal of Physics and Chemistry of Solids* **2003**, *64* (9–10), 1791–1796. [https://doi.org/10.1016/S0022-3697\(03\)00201-4](https://doi.org/10.1016/S0022-3697(03)00201-4).
- (15) Bouttemy, M.; Tran-Van, P.; Gerard, I.; Hildebrandt, T.; Causier, A.; Pelouard, J. L.; Dagher, G.; Jehl, Z.; Naghavi, N.; Voorwinden, G.; Dimmler, B.; Powalla, M.; Guillemoles, J. F.; Lincot, D.; Etcheberry, A. Thinning of CIGS Solar Cells: Part I: Chemical Processing in Acidic Bromine Solutions. *Thin Solid Films* **2011**, *519* (21), 7207–7211. <https://doi.org/10.1016/j.tsf.2010.12.219>.
- (16) Jehl Li-Kao, Z.; Naghavi, N.; Erfurth, F.; Guillemoles, J. F.; Gérard, I.; Etcheberry, A.; Pelouard, J. L.; Collin, S.; Voorwinden, G.; Lincot, D. Towards Ultrathin Copper Indium Gallium Diselenide Solar

- Cells: Proof of Concept Study by Chemical Etching and Gold Back Contact Engineering. *Prog. Photovolt: Res. Appl.* **2012**, *20* (5), 582–587. <https://doi.org/10.1002/pip.2162>.
- (17) Mousel, M.; Redinger, A.; Djemour, R.; Arasimowicz, M.; Valle, N.; Dale, P.; Siebentritt, S. HCl and Br₂-MeOH Etching of Cu₂ZnSnSe₄ Polycrystalline Absorbers. *Thin Solid Films* **2013**, *535*, 83–87. <https://doi.org/10.1016/j.tsf.2012.12.095>.
- (18) Miyazaki, H.; Aono, M.; Kishimura, H.; Katagiri, H. Surface Etching of CZTS Absorber Layer by Br-Related Solution. *physica status solidi c* **2015**, *12* (6), 741–744. <https://doi.org/10.1002/pssc.201400274>.
- (19) Yan, C.; Sun, K.; Liu, F.; Huang, J.; Zhou, F.; Hao, X. Boost Voc of Pure Sulfide Kesterite Solar Cell via a Double CZTS Layer Stacks. *Solar Energy Materials and Solar Cells* **2017**, *160*, 7–11. <https://doi.org/10.1016/j.solmat.2016.09.027>.
- (20) Giraldo, S.; Saucedo, E.; Neuschitzer, M.; Oliva, F.; Placidi, M.; Alcobé, X.; Izquierdo-Roca, V.; Kim, S.; Tampo, H.; Shibata, H.; Pérez-Rodríguez, A.; Pistor, P. How Small Amounts of Ge Modify the Formation Pathways and Crystallization of Kesterites. *Energy & Environmental Science* **2018**, *11* (3), 582–593. <https://doi.org/10.1039/C7EE02318A>.
- (21) Dimitrievska, M.; Oliva, F.; Guc, M.; Giraldo, S.; Saucedo, E.; Pérez-Rodríguez, A.; Izquierdo-Roca, V. Defect Characterisation in Cu₂ZnSnSe₄ Kesterites via Resonance Raman Spectroscopy and the Impact on Optoelectronic Solar Cell Properties. *J. Mater. Chem. A* **2019**, *7* (21), 13293–13304. <https://doi.org/10.1039/C9TA03625C>.
- (22) Jehl, Z.; Erfurth, F.; Naghavi, N.; Lombez, L.; Gerard, I.; Bouttemy, M.; Tran-Van, P.; Etcheberry, A.; Voorwinden, G.; Dimmler, B.; Wischmann, W.; Powalla, M.; Guillemoles, J. F.; Lincot, D. Thinning of CIGS Solar Cells: Part II: Cell Characterizations. *Thin Solid Films* **2011**, *519* (21), 7212–7215. <https://doi.org/10.1016/j.tsf.2010.12.224>.
- (23) Kim, S.-Y.; Kim, S.-H.; Hong, S.; Son, D.-H.; Kim, Y.-I.; Kim, S.; Ahn, K.; Yang, K.-J.; Kim, D.-H.; Kang, J.-K. Secondary Phase Formation Mechanism in the Mo-Back Contact Region during Sulfo-Selenization Using a Metal Precursor: Effect of Wettability between a Liquid Metal and Substrate on Secondary Phase Formation. *ACS Appl. Mater. Interfaces* **2019**, *11* (26), 23160–23167. <https://doi.org/10.1021/acsami.9b03969>.
- (24) López-Marino, S.; Sánchez, Y.; Placidi, M.; Fairbrother, A.; Espindola-Rodríguez, M.; Fontané, X.; Izquierdo-Roca, V.; López-García, J.; Calvo-Barrio, L.; Pérez-Rodríguez, A. ZnSe Etching of Zn-Rich Cu₂ZnSnSe₄: An Oxidation Route for Improved Solar-Cell Efficiency. *Chemistry—A European Journal* **2013**, *19* (44), 14814–14822.
- (25) Wagner, C.; Riggs, W.; Davis, L.; Moulder, J.; Muilenberg, G. Handbook of X-Ray Photoelectron Spectroscopy. 1979. *Eden, MN Perkin-Elmer Corp., Physical Electronics Division*.
- (26) Kim, S.; Park, J.-S.; Walsh, A. Identification of Killer Defects in Kesterite Thin-Film Solar Cells. *ACS Energy Letters* **2018**, *3* (2), 496–500.
- (27) Becerril-Romero, I.; Acebo, L.; Oliva, F.; Izquierdo-Roca, V.; López-Marino, S.; Espíndola-Rodríguez, M.; Neuschitzer, M.; Sánchez, Y.; Placidi, M.; Pérez-Rodríguez, A.; Saucedo, E.; Pistor, P. CZTSe Solar Cells Developed on Polymer Substrates: Effects of Low-Temperature Processing. *Progress in Photovoltaics: Research and Applications* **2018**, *26* (1), 55–68. <https://doi.org/10.1002/pip.2945>.
- (28) Chen, S.; Wang, L.-W.; Walsh, A.; Gong, X. G.; Wei, S.-H. Abundance of CuZn + SnZn and 2CuZn + SnZn Defect Clusters in Kesterite Solar Cells. *Appl. Phys. Lett.* **2012**, *101* (22), 223901. <https://doi.org/10.1063/1.4768215>.
- (29) Jehl, Z.; Bouttemy, M.; Lincot, D.; Guillemoles, J. F.; Gerard, I.; Etcheberry, A.; Voorwinden, G.; Powalla, M.; Naghavi, N. Insights on the Influence of Surface Roughness on Photovoltaic Properties of State of the Art Copper Indium Gallium Diselenide Thin Films Solar Cells. *Journal of Applied Physics* **2012**, *111* (11), 114509. <https://doi.org/10.1063/1.4721648>.

Supporting Information

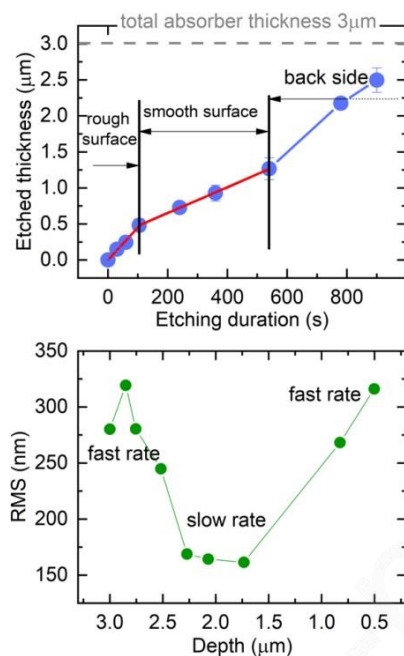


Figure SI 1 Etching rate (top) and surface RMS (bottom) of etched kesterite films.

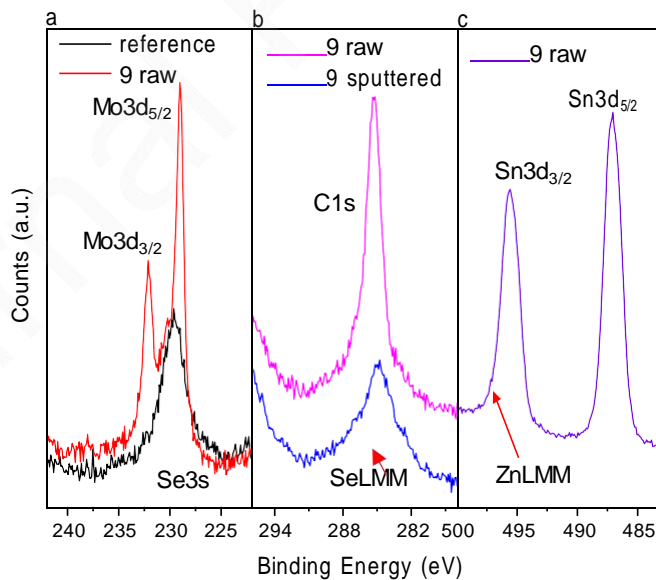


Figure SI 2 XPS Signals from orbitals and auger lines of different elements present in the samples that can overlap when analysing by X-ray source Al K α line: Mo3d with Se3s, C1s with SeLMM and Sn3d_{3/2} with ZnLMM in a, b and c respectively, in sample raw and sputtered and the reference sample as example.

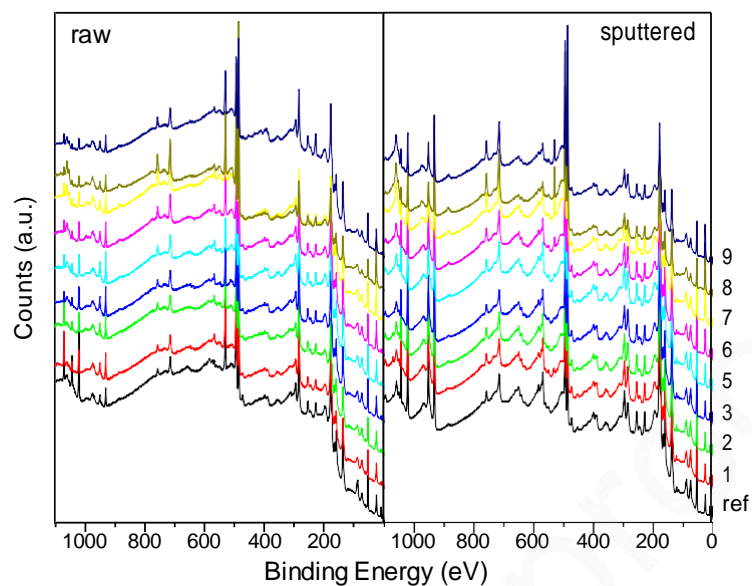


Figure SI 3 Survey XPS spectra for all the set of etched samples as presented (raw) and sputtered.

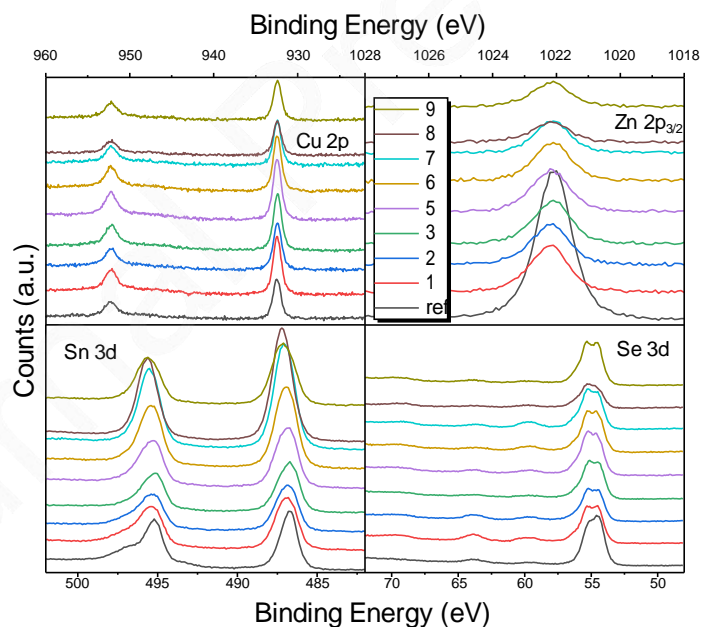


Figure SI 4 High-resolution XPS spectra for the main orbitals of the CZTSe elements in all the set samples as presented (raw).

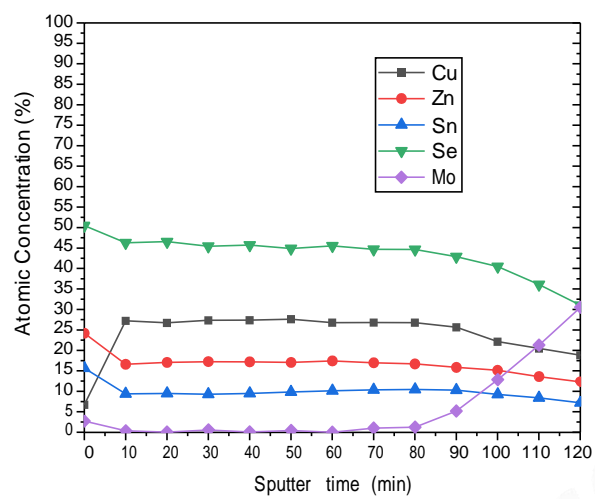


Figure SI 5 Atomic concentration profile obtained by XPS for the reference sample.

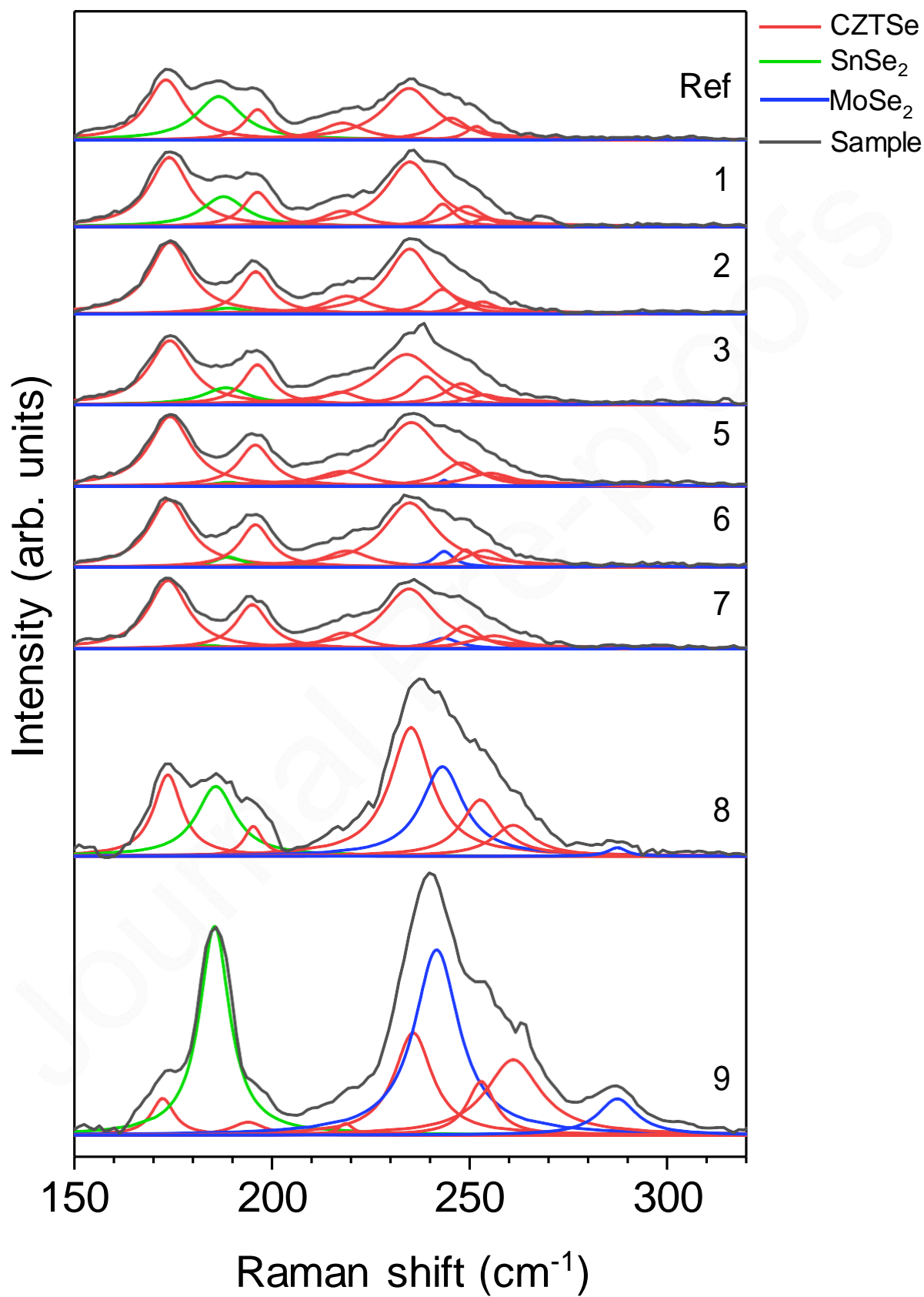


Figure SI 6 Raman spectra fitting deconvolution using Lorentzian curves of the spectra acquired under 325 nm excitation wavelength for the different etching times samples.

Journal Pre-proofs

Kunal J. Tiwari – *Methodology, Investigation*

Robert Fonoll – *Investigation, Data Curation, Visualization*

Sergio Giraldo – *Investigation, Validation*

Lorenzo Calvo Barrio – *Investigation, Data Curation, Visualization*

Victor Izquierdo Roca – *Investigation*

Marcel Placidi – *Writing Review and editing*

Yudania Sanchez – *Resources*

Alejandro Perez Rodriguez – *Funding acquisition, Supervision*

Edgardo Saucedo – *Funding acquisition, Supervision*

Zacharie Jehl Li-Kao – *Conceptualization, Methodology, Investigation, Data Curation, Visualization, Supervision, Writing Original draft and Review and editing*

Declaration of interests

The authors declare that they have no known competing financial interests or personal relationships that could have appeared to influence the work reported in this paper.

The authors declare the following financial interests/personal relationships which may be considered as potential competing interests:

Zacharie Jehl Li-Kao

A handwritten signature in black ink, appearing to be 'ZJL' with a horizontal line underneath.

Journal Pre-proofs

- First ever depth profiling of defects limiting the efficiency on kesterite solar cells.
- Elemental depth composition showing a greater accuracy than regular approaches based on physical etching of the films.
- Direct observation of secondary phase segregation towards the back interface of kesterite absorbers.
- Versatile and simple method combining chemical etching and surface characterization, possibly to a various range of thin film absorbers (material agnostic).

Journal Pre-proofs